



Bimetallic Ru/Ni supported catalysts for the gas phase hydrogenation of acetonitrile

P. Braos-García, C. García-Sancho, A. Infantes-Molina, E. Rodríguez-Castellón, A. Jiménez-López*

Departamento de Química Inorgánica, Cristalografía y Mineralogía (Unidad Asociada al ICP-CSIC), Facultad de Ciencias, Universidad de Málaga, Campus de Teatinos, 29071 Málaga, Spain

ARTICLE INFO

Article history:

Received 21 December 2009
Received in revised form 16 March 2010
Accepted 30 March 2010
Available online 4 April 2010

Keywords:

Gas phase acetonitrile hydrogenation
Supported nickel-ruthenium bimetallic catalysts
Mesoporous silica
SBA-15

ABSTRACT

A family of bimetallic Ni-Ru catalysts supported on a mesoporous SBA-15 silica was prepared by conventional impregnation method, with constant metal molar loadings, but varying Ni/(Ni + Ru) atomic ratios. The corresponding Ni and Ru monometallic catalysts were also prepared for comparison. These catalysts were characterized by XRD, N₂ adsorption–desorption at –196 °C, TEM, XPS, H₂-TPR, chemisorption of H₂ at r.t., H₂-TPD and NH₃-TPD techniques. Finally, they were also tested in the hydrogenation of acetonitrile reaction, in the gas phase and at atmospheric pressure. Acetonitrile conversion values depended on the Ni/(Ni + Ru) composition of the bimetallic catalysts. Ru-rich bimetallic catalysts exhibited acetonitrile conversion values higher than that of pure Ni one; thus, although selectivity patterns remained almost unchanged, primary amine yields were increased. These higher conversion values resulted as a consequence of enhanced specific activity of Ni⁰ atoms, attributable to a strong interaction between both metals, Ni and Ru, likely because NiRu alloy nanoparticles were formed.

© 2010 Elsevier B.V. All rights reserved.

1. Introduction

Lower alkylamines ranging from C₂ to C₅ are used as solvents, agrochemicals, surfactants, water treatment chemicals, and pharmaceuticals [1]. One important industrial route to amines is based in the hydrogenation of nitriles. The reaction selectivity is of great importance, particularly for the production of primary amines, often the most industrially desired products. Due to the high reactivity of partially hydrogenated reaction intermediates, i.e., imines or Schiff bases, a conventional hydrogenation process leads to a mixture that also contains secondary and tertiary amines [2]. The metal employed as catalyst is the most important factor in determining the selectivity for the hydrogenation of nitriles. For the production of primary amines, the nickel-based catalysts are commonly used [3–5]. In the case of nickel supported catalysts, also the support nature has been proved to exert a strong influence on the selectivity [6–9].

The knowledge of the mechanism of the hydrogenation reaction is a key point when attempting to rationalize the formation of undesired products, in order to eliminate them, or, at least, reduce them. Dallons et al. proposed that all reactions leading to amines occur exclusively on the catalyst's surface [10] and Huang and Sachtler have shown that the selectivity to a particular amine is dominantly

determined by the propensity of the metals to form multiple bonds: after deuteration of acetonitrile experiments they have proposed that intermolecular hydrogen transfer from the α -methylene group of one adsorbed nitrile to the strong metal=N bond of another adsorbed species is responsible for amine formation [11,12]. On this basis, they propose that, among the transition metal catalysts, Ru displays the highest selectivity to primary amine, while over Pd and Pt, secondary and tertiary amines are preferentially formed; the selectivity of Ni and Rh is between these extremes [5].

In any case, the adsorbed nitriles and their intermediates are active species that react with each other and controlling their interactions is key to govern the overall selectivity of the reaction. In this sense, a number of studies have dealt with the performance of bimetallic catalysts [13–15], since the range of properties of metallic systems can be greatly extended by taking mixtures of elements to generate compounds and alloys. Our group has been working with nickel catalysts in the hydrogenation of acetonitrile in the gas phase, finding highly active catalysts with high selectivity towards ethylamine when the metal is supported on a silica carrier [9]. Thus, given that Ru catalysts have been proposed to be even more selective towards the primary amine than Ni ones, although much less active, the aim of the present work is to test the performance of bimetallic Ni-Ru catalysts supported on high surface mesoporous silica. In this sense, nanoalloys can be generated in a variety of media, such as immobilized on surfaces, or inside pores. One of the major reasons for interest in alloy nanoparticles is the fact that their chemical and physical properties may be tuned by varying the

* Corresponding author. Tel.: +34 952131876; fax: +34 952137534.
E-mail address: ajimenezl@uma.es (A. Jiménez-López).

composition and atomic ordering as well as the size of clusters. In fact, nanoalloys may display *magic compositions*, i.e., compositions at which the alloy nanoclusters present a special stability. They may also display properties which are distinct from the corresponding bulk alloys due to finite size effects, e.g., there are examples of pairs of elements which are immiscible in the bulk but readily mix in finite clusters, such as iron and silver [16]. In the case of Ni and Ru system, although it has a positive heat of formation of +1 kJ/mol and is essentially equilibrium immiscible (in fact, in its equilibrium phase diagram, there is no any alloy phase over the whole composition range) [17], many authors have described Ni-Ru bimetallic clusters or alloys [18,19]. Finally, it is well known that acidic oxide supports originate strong metal-support interactions leading to metal segregation on bimetallic catalysts [20,21]. To avoid such effects, as well as secondary reactions leading to higher amines different from ethylamine, which are favoured by the surface acidity of supports, we have selected a high surface area, but very low acidity mesoporous silica. Thus, our group has recently published the synthesis and characterization of a well ordered mesoporous silica, of the SBA-15 type, with such desired characteristics [22]. It was therefore the aim of this study to investigate the influence of Ru atoms on the catalytic performance of Ni supported on a silica carrier, in the hydrogenation of acetonitrile in the gas phase, by progressively substituting Ni atoms by Ru ones, that is, by preparing Ni-Ru bimetallic catalysts.

2. Experimental

2.1. Materials

The mesoporous silica SBA-15 material was prepared by following the method reported by Gómez-Cazalilla et al. [22]. The resulting solid after calcination at 550 °C for 6 h (10 °C min⁻¹ heating rate), was pelletized so that a sieve fraction 0.3–0.4 mm was used afterwards.

A series of bimetallic supported Ni-Ru catalysts was prepared using the incipient wetness impregnation method of pelletized support. Aqueous solutions of Ni and Ru, of required concentrations, were employed in such a way that a constant loading of metallic moles per gram of solid, 500 μmol M g⁻¹ (where M = Ni + Ru), resulted with varying Ni/(Ni + Ru) molar ratios. Towards this end, the support was impregnated with an aqueous solution of Ni(II) citrate [23], air dried overnight at 60 °C, and calcined to 450 °C for 2 h (1 °C min⁻¹ heating rate), in order to eliminate the organic ligands. Afterwards, ruthenium was added by a subsequent impregnation process with an aqueous solution of RuCl₃·nH₂O (~41 wt% Ru, from Fluka). The resulting solid was air dried at 60 °C for 1 day, giving rise to the corresponding catalyst precursor. Monometallic Ni and Ru precursors were also prepared in analogous manner, with 3 wt% of Ni (500 μmol g⁻¹), and 1.7 wt% of Ru (167 μmol g⁻¹), respectively.

The catalysts were obtained by treating the precursors with an He flow (60 ml min⁻¹) at 100 °C, for 30 min, and lately cooled down to room temperature; to be subsequently reduced in flowing H₂ (60 ml min⁻¹) from room temperature to and kept at 400 °C for 30 min (10 °C min⁻¹ of heating rate).

The catalysts will be referred to as Ni and Ru, for monometallic nickel and ruthenium, respectively, and NiRu_x, for bimetallic ones, where x is the Ni/(Ni + Ru) molar ratio. The corresponding compositions are compiled in Table 1.

2.2. Characterization of catalysts

X-ray photoelectron spectra were collected using a Physical Electronics PHI 5700 spectrometer with either non-monochromatic Mg Kα (1253.6 eV) or Al Kα radiation (1486.6 eV) and with a multi-channel detector *Electronics 80-365B*. Core level spectra of samples were recorded in the constant pass energy mode at 29.35 eV, using a 720 μm diameter analysis area. All the binding energies (B.E.) were referenced to the C 1s peak of adventitious carbon at 284.8 eV, with an uncertainty of ±0.1 eV. A PHI ACCESS ESCA-V6.0 F software package was used for data acquisition and analysis. A Shirley-type background was subtracted from the signals. Recorded spectra were always fitted using Gaussian-Lorentzian functions in order to determine the binding energy of the different element core levels more accurately.

TEM micrographs of the catalysts were obtained with a *Philips CM 200 Supertwin-DX4* high resolution transmission electron microscope. Once the samples were reduced, they were kept in cyclohexane. For sample preparation, a drop of these suspensions was dispersed on a Cu grid.

Powder X-ray diffraction patterns were collected by using a *Phillips Xpert PRO MPD* diffractometer, using Cu Kα1 radiation, provided with a Ge(1 1 1) monochromator.

Nitrogen physisorption measurements were performed at -196 °C with a *Micromeritics ASAP 2020* apparatus. Prior to analysis, the samples were outgassed at 200 °C and 10⁻² Pa overnight. Surface areas were determined by using the Brunauer-Emmet-Teller equation [24] and a nitrogen molecule cross-section of 13.5 Å² [25,26].

Hydrogen temperature-programmed reduction (H₂-TPR) experiments were carried out to 0.080 g of catalyst precursor, previously treated with a He flow (35 ml min⁻¹) at 100 °C for 30 min. After cooling to room temperature, the H₂ consumption was studied between this temperature and 800 °C, by using an Ar/H₂ flow (48 ml min⁻¹, 10 vol% of H₂) and under a heating rate of 10 °C min⁻¹. Water and/or hydrogen chloride formed in the reduction reaction were removed by passing the outcoming flow through a solid CaO trap and a cold finger (-80 °C). The H₂ consumption was measured with an on-line gas chromatograph (*Shimadzu GC-14A*) provided with a TCD.

Temperature-programmed desorption of H₂ (H₂-TPD) was carried out placing 0.300 g of catalyst precursor in U tube reactor

Table 1

Composition, textural and acidic properties (from NH₃-TPD experiments) of Ni, Ru, and NiRu_x bimetallic catalysts., as well as those corresponding to the support.

Catalyst	Ni (wt%)	Ru (wt%)	μmol Ni g ⁻¹	μmol Ru g ⁻¹	S _{BET} (m ² g ⁻¹)	V _p (cm ³ g ⁻¹) ^a	d _p (nm) ^b	μmol NH ₃ g ⁻¹
SBA-15 (pelletized)					310	0.34	4.3	99
Ni	3.0	0	508	0	257	0.28	4.4	366
NiRu0.89	2.6	0.6	446	55	309	0.34	4.4	275
NiRu0.80	2.3	1.0	399	99	296	0.32	4.3	262
NiRu0.67	1.9	1.7	327	163	302	0.32	4.2	738
NiRu0.50	1.4	2.4	242	241	270	0.29	4.3	575
NiRu0.33	0.9	3.2	159	318	327	0.34	4.2	883
Ru	0	1.7	0	165	307	0.33	4.3	504

^a V_p mesoporous volume estimated from the N₂ adsorption isotherm at P/P₀ = 0.95.

^b By 4 V_p/A method, where A is the BET surface area.

where it was firstly reduced *in situ*. The obtained catalyst was purged with a He flow (50 ml min⁻¹) at the reduction temperature for 15 min, cooled down to 135 °C (chemisorption temperature), and then put in contact with flowing H₂ (30 ml min⁻¹) for 1 h, and lately cooled to r.t. under the same H₂ flow. After cleaning with Ar (35 ml min⁻¹), the H₂-TPD was performed by heating (15 °C min⁻¹) from r.t. to 800 °C. The evolved H₂ was analysed by an on-line chromatograph (*Shimadzu GC-14A*) provided with a TCD. A cold finger (-80 °C) was employed as water trap. The hydrogen consumed (TPR) or desorbed (TPD) was quantified by calibration with pure CuO as reference compound (Aldrich), assuming a total reduction of CuO to Cu⁰.

Hydrogen chemisorption measurements at r.t. were carried out in a *Micromeritics ASAP 2010C* equipment, under static volumetric conditions. 0.200 g of catalyst precursor was reduced *in situ*. After reduction, the sample was evacuated for 12 h at the reduction temperature and cooled under vacuum (1.3 × 10⁻² Pa) to the analysis temperature, 35 °C. The reported hydrogen uptake values were taken from the volume difference between two hydrogen adsorption isotherms extrapolated to zero pressure (strongly adsorbed hydrogen), the second one measured after an evacuation at the analysis temperature. A H:M (M=Ni and/or Ru) atomic ratio of 1 was used for calculations.

Ammonia thermoprogrammed desorption (NH₃-TPD) profiles of catalysts were obtained by placing 0.080 g of catalyst precursor into a tubular reactor, where it was firstly reduced *in situ*. After cleaning with He (35 ml min⁻¹) from r.t. to 400 °C (10 min), and cooling to 100 °C, the adsorption of ammonia (5 min) at this temperature was performed. An He flow (35 ml min⁻¹) was next passed to eliminate the physisorbed ammonia. Thermoprogrammed desorption was then carried out by heating the samples from 100 °C to the reduction temperature, 400 °C, at a heating rate of 10 °C min⁻¹. The evolved ammonia was analysed by on-line gas chromatograph (*Simadzu GC-14A*) provided with a TCD. In order to quantify the amount of ammonia desorbed, the equipment was previously calibrated by measuring the corresponding signals of the thermal decomposition of known amounts of hexaamminenickel(II) chloride [Ni(NH₃)₆]Cl₂, supplied by Aldrich.

2.3. Catalytic test

The gas phase hydrogenation of acetonitrile was performed in a flow system operating at atmospheric pressure. A tubular Pyrex reactor (27 cm length, 7 mm o.d. and 3.6 mm i.d.) was used. Prior to any measurement, 0.030 g of catalyst precursor were reduced *in situ*. Afterwards, a hydrogen flow, previously bubbled through a saturator containing acetonitrile (Aldrich, HPLC grade), was introduced into the reactor. The resulting feed contained 4.8 mol% of acetonitrile (total flow, 146 ml min⁻¹; H₂:CH₃CN molar ratio = 20). The reactant and the products were analysed by means of an on-line chromatograph (*Shimadzu GC-14A*) equipped with a *TRB-14* column and a FID. Tests were performed at 135 °C.

The conversion is defined as

$$\text{Conversion(mol\%)} = 100 \times \frac{(\text{CH}_3\text{CN}_{\text{in}} - \text{CH}_3\text{CN}_{\text{out}})}{\text{CH}_3\text{CN}_{\text{in}}}$$

The selectivities have been calculated from peak areas by considering the different sensitivity factors in the flame ionisation detector. The selectivity for the product *i* is defined as

$$\text{Selectivity}_i(\text{mol\%}) = 100 \times \frac{(\text{corrected area})_i}{\text{sum of all corrected areas}}$$

A series of preliminary experiments was previously carried out in order to rule out the existence of diffusional limitations under the experimental conditions used.

3. Results and discussion

3.1. Support

The characteristics of the SBA-15 support employed have been described elsewhere [22]. It is a silica formed by hexagonal array of mesopores of ca. 40 Å in diameter, with pore walls thickness of ~53 Å. These parameters have been further confirmed by XRD patterns and TEM images of reduced NiRu bimetallic catalysts, corroborating the high framework stability of this solid during catalysts preparation. With a BET surface area of 310 m² g⁻¹, and a pore volume of 0.34 cm³ g⁻¹ (see Table 1), this pelletized mesoporous silica exhibits very low acidity, as measured in NH₃-TPD experiments (Table 1).

3.2. XRD

X-ray diffractograms at high angles of the catalyst precursors display only very weak and broad reflections at 2θ = 37.3°, 43.3° and 62.8° (Fig. 1a), corresponding to very small NiO particles, that become less intense as the nickel content decreases. Since hydrated ruthenium chlorides and/or oxychlorides are amorphous species, no signal can be seen that could be attributable to any Ru compound [27]. After reduction (Fig. 1b) a broad but more intense peak appears at 2θ = 44.5°, which is attributed to the presence of Ni⁰ particles, and indicates that formation of the metallic phase has occurred in some extent. So, when compared to the pure Ni catalyst, it seems that the addition of small amounts of Ru has led to a higher amount of Ni⁰ crystallites and/or a decrease in the Ni⁰ dispersion (as will be discussed later in Section 3.5); this phenomenon being especially important for catalyst NiRu0.80. On the other hand, peaks corresponding to Ru⁰ are more difficult to appreciate: they would be expected to appear at 2θ = 38.8°, 42.2° and 44.0°. Given the low intensity and broadness of the signals, the most intense peak, at 44.0°, would overlap with that of Ni⁰ at 44.5°. Only for samples with Ni/(Ni + Ru) equal or lower than 0.67, two small reflection lines seem to appear at 38.4° and 42.2°, indicating the presence of very small and dispersed Ru⁰ particles. For the pure Ru catalyst, no peaks can be detected, what can be due to a very low amount of Ru⁰ (low degree of reduction for this catalyst, as it will be discussed later) and/or the very small size of the metallic particles.

3.3. Textural parameters

N₂ adsorption-desorption isotherms of the support hardly changed upon Ni and Ru metals incorporation and reduction (Fig. 2), that is to say, neither a shift of the capillary condensation nor a decrease of the average pore size occurred. Only the values of surface area slightly reduced for pure Ni and NiRu0.50 catalysts (Table 1). So, some pore blocking must occurred in these two catalysts, probably because a greater portion of metal loadings has been introduced in the channels of the support or is covering the entrance of the pores.

3.4. TEM

TEM analysis of the pure Ni catalyst shows that no large nickel particles have been formed; indeed, no particles larger than ~3.5 nm can be visualized, being homogeneously distributed in the silica matrix (Fig. 3a). It is known that the nickel citrate precursor leads, after calcination, to the formation of small nickel oxide particles with high dispersion [23]. The metal-support interaction prevents Ni⁰ particles agglomeration upon reduction treatment. The small particle sizes observed are in agreement with the fact that they are limited by the dimensions of the tubular pores where they have been formed.

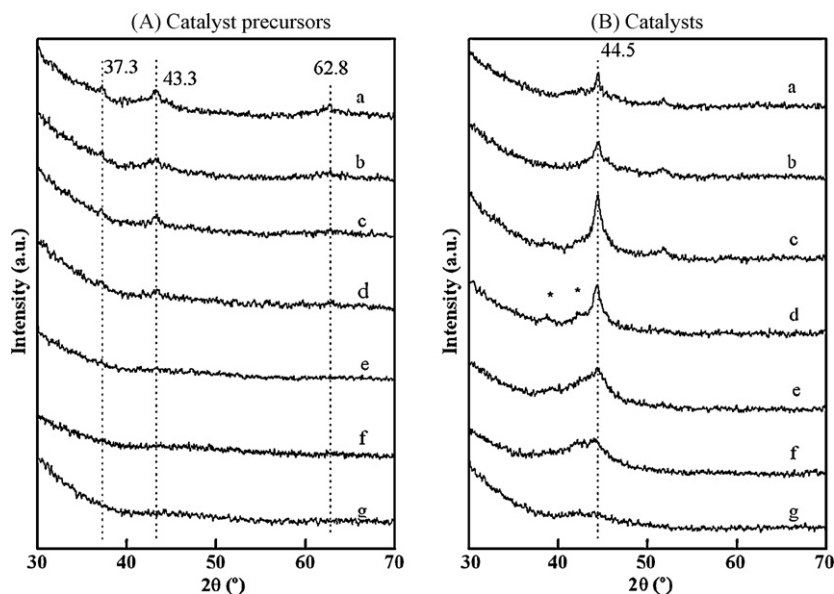


Fig. 1. XRD patterns at high angle for catalyst precursors (A) and reduced catalysts (B): (a) Ni, (b) NiRu0.89, (c) NiRu0.80, (d) NiRu0.67, (e) NiRu0.50, (f) NiRu0.33, and (g) Ru; (*) 38.8° and 42.2°.

The same fact can be said about the pure Ru catalyst (Fig. 3b), where the micrograph even shows that metallic particles are aligned, being a demonstration that most of these are inside of the silica mesopores.

By contrast, the situation is very different for bimetallic NiRuX catalysts. In these samples, the metallic particles are distributed heterogeneously into two manners: (i) those with small sizes, interacting with the support, and mainly located inside the silica pores; and (ii) those with large metallic particle sizes, forming aggregates, which are situated on the external surface of the support, and scarcely interacting with this. Furthermore, the proportion of these two kinds of metallic particles varies from one catalyst to another depending on the Ni/(Ni + Ru) atomic ratio. Thus, for NiRu0.89 catalyst, we can find zones of support which contain small particles (not greater than 4 nm in diameter) (Fig. 3c); on the other hand, large particles or particle aggregates can also easily be found (Fig. 3d).

For NiRu0.80 catalyst, the support hardly contains dispersed particles (Fig. 3e). Instead, large particles or aggregates are the dominant form for the metallic particles (Fig. 3f). This is in agreement

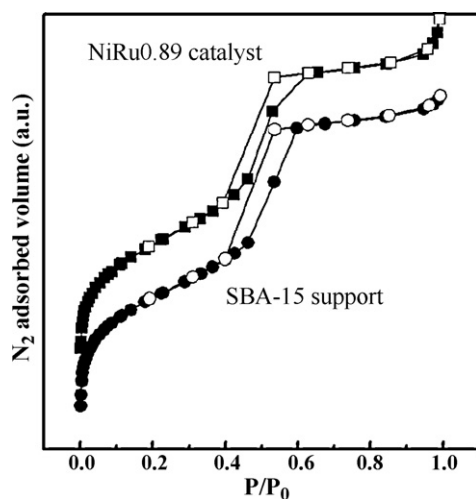


Fig. 2. N₂ adsorption (solid symbols) and desorption (open symbols) isotherms for SBA-15 carrier and bimetallic NiRu0.89 catalyst.

with increased intensity of Ni⁰ peaks in XRD patterns, as has been already discussed, where NiRu0.80 catalyst exhibited the peaks of Ni⁰ with maximum intensity.

By further decreasing the Ni/(Ni + Ru) molar ratio, the same feature is observed, although the proportion of both kinds of metallic particles seems to vary. In general, small particles are more abundant while the large ones are more difficult to find (see Fig. 4). So, this suggests that a higher metallic dispersion has been achieved on increasing the amount of Ru. For all samples, the size of small metallic particles is never greater than 5 nm, and again, they seem to form rows, indicating that they are mainly located inside of the tubular pores of the support.

3.5. H₂-TPR

Fig. 5 shows the TPR profiles of supported monometallic and bimetallic catalyst precursors in flowing hydrogen.

The H₂-TPR profile of the pure supported NiO shows a sharp peak, centred at 316 °C, and a very broad one, centred at 550 °C. This high temperature peak originated from the slow reduction of small nickel oxide particles, strongly interacting with the silica framework, or even Ni²⁺ ions interacting with Si–O[−] sites. As regards to the low temperature peak, it is normally attributed to the presence of very small NiO particles, well dispersed and scarcely interacting with the support [23].

As regards to the pure Ru unreduced catalyst, the profile shows two reduction peaks, centred at 134 °C and 300 °C, respectively. For comparison, a TPR experiment was carried out employing the amount of pure RuCl₃·xH₂O salt that contains the same amount of Ru moles as pure Ru catalyst. The corresponding TPR profile is also shown in Fig. 5, and indicates that the reduction process is complex, with several narrow peaks occurring between 180 and 278 °C, the most intense one centred at 200 °C, in accordance with the results published by others [28]. Furthermore, the H₂ consumption is intermediate between the values expected for the reduction of Ru(III) and Ru(IV). This result is in agreement with the fact that our starting ruthenium salt, the commercially hydrated ruthenium trichloride, is actually a mixture of different ruthenium compounds, presumably mostly in the +IV oxidation state [27] (calculations indicate that 68% of Ru is in the +IV oxidation state). None of these peaks are present in our pure Ru catalyst precursor, indicating that

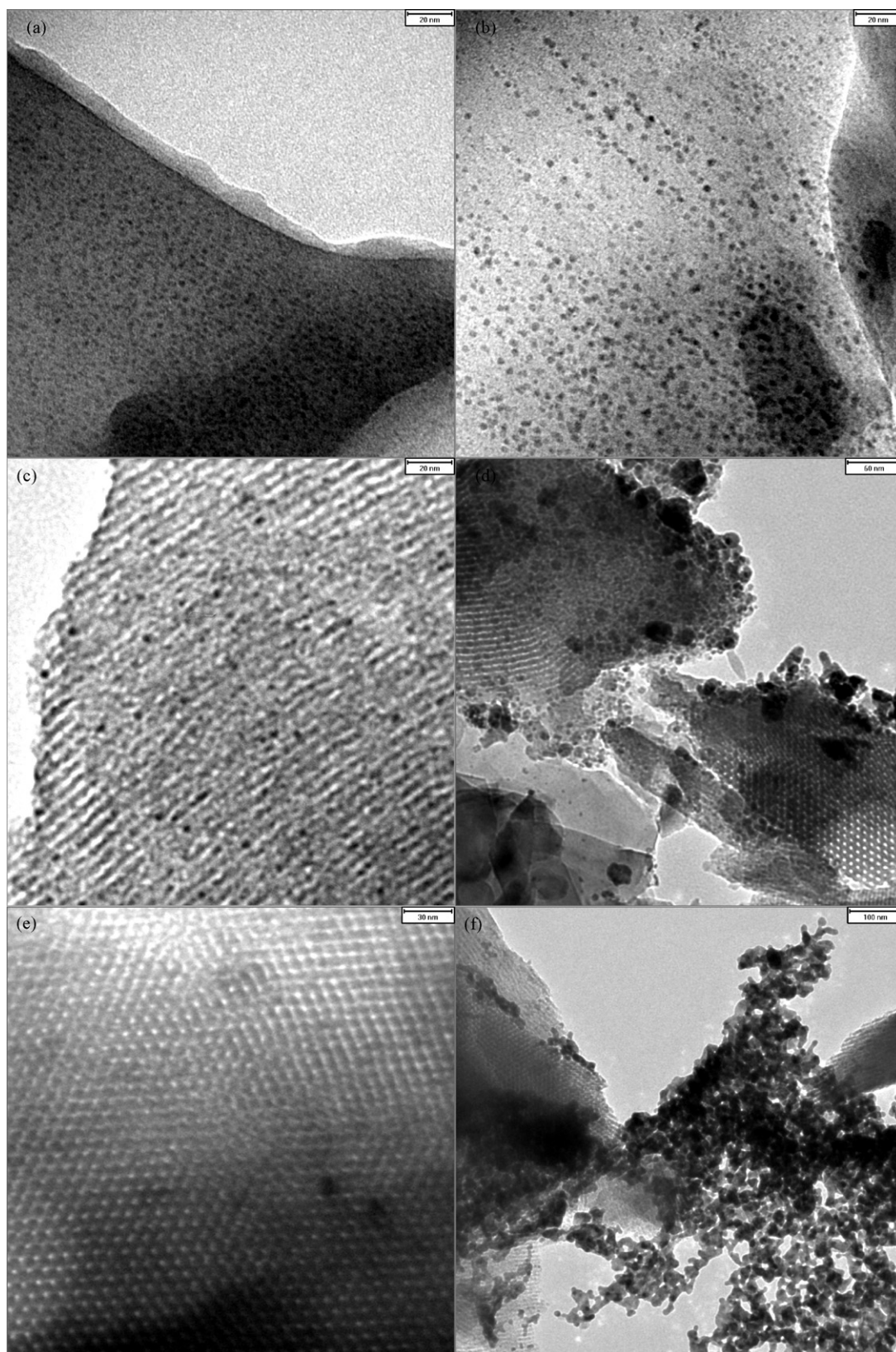


Fig. 3. TEM micrographs for reduced catalysts (a) Ni, (b) Ru, (c) NiRu0.89, small, well-dispersed metallic particles on the support, (d) NiRu0.89, large particles, (e) NiRu0.80, support, and (f) NiRu0.80, large particles, segregated from the support.

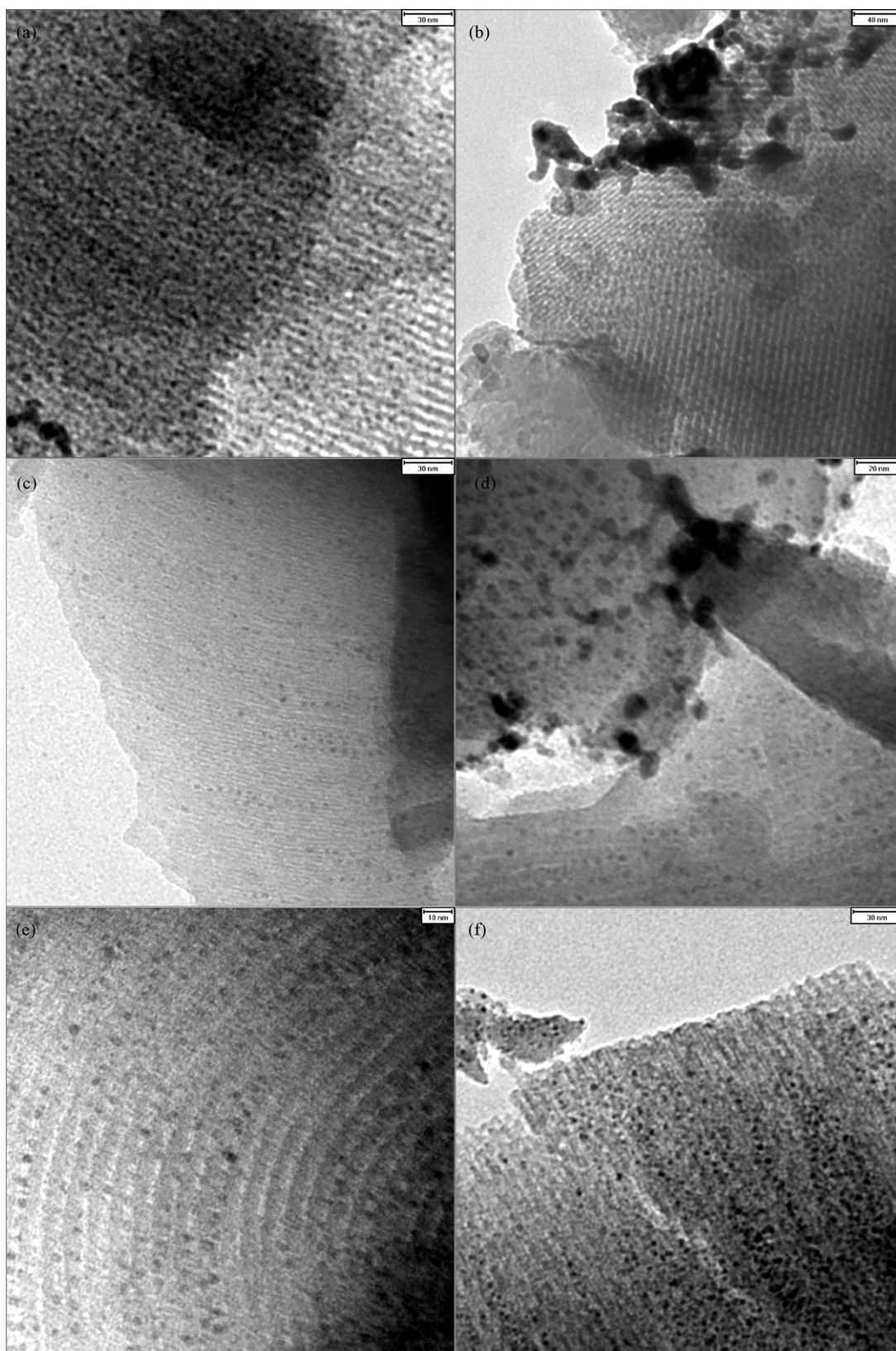


Fig. 4. TEM micrographs for reduced catalysts (a) NiRu0.67, small, well-dispersed metallic particles on the support, (b) NiRu0.67, large particles, (c) NiRu0.50, small, well-dispersed metallic particles on the support, (d) NiRu0.50, large particles, segregated from the support, and (e) and (f) NiRu0.33, small, well-dispersed metallic particles on the support.

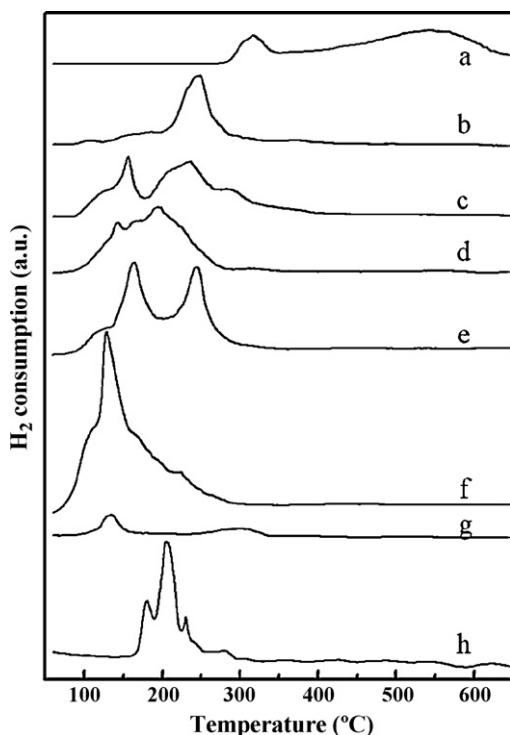


Fig. 5. H₂-TPR profiles of catalyst precursors: (a) Ni, (b) NiRu0.89, (c) NiRu0.80, (d) NiRu0.67, (e) NiRu0.50, (f) NiRu0.33, (g) Ru, and (h) pure RuCl₃·*n*H₂O.

interaction of RuCl₃·*x*H₂O with the silica support greatly affects its reducibility. The low temperature peak has been reported by a number of authors [29,30], and can be assigned to the presence of very small well-dispersed particles of the ruthenium salt, which would be more reducible than unsupported ones. As regards to the high temperature peak, some authors have attributed it to the reduction of RuO_{*x*}Cl_{*y*} species, containing Ru(IV) [31]. These species are present in our materials, as pointed out by XPS data (see later). Furthermore, this peak can also be due to ruthenium ions strongly interacting with the support, likely with Si–O[–] sites, as proposed by Eliche-Quesada et al. [30]. The percentage of Ru reduction estimated at 400 °C is 33% (Table 2). This low reduction percentage clearly corroborates the strong interactions between ruthenium species and the support.

The reduction patterns of NiRu_{*x*} bimetallic catalyst precursors are clearly different from those of the monometallic ones of ruthenium and nickel. The reduction process begins at temperatures as low as 100 °C for all the samples and finishes below 400 °C, showing a very complex pattern, with several overlapping peaks

whose maxima appear at temperatures between 100 and 290 °C. So, the mixture of the supported solids, NiO and RuCl₃, enhances the reducibilities of both metal cations. This effect has also been reported by other authors [32], and has been attributed to the intimate contact of Ru species with the Ni ones. Furthermore, exchange Si–O[–] sites are possibly occupied by Ni²⁺ species when the Ru salt is added. This would explain the low temperature of reduction of Ru species to form Ru⁰, and, more importantly, these Ru⁰ species are capable of chemisorbing hydrogen molecules and supply the hydrogen active species to nickel and/or other ruthenium species, by hydrogen spillover, either directly or through the support. Moreover, this ease of reduction would also explain why we do not find surface residual chloride species in our catalysts by XPS analysis, as will be discussed in Section 3.8. On the other hand, the simultaneous reduction of both metals, as well as the presence of several overlapping peaks, suggest the formation of one or more Ni/Ru alloys, as reported by other authors [33,34]. Quantification of these curves has been carried out assuming the total reduction of ruthenium species. For Ni-rich samples, NiRu0.89 and NiRu0.80, this hypothesis seems very likely, given that TEM micrographs suggest that the interaction of Ru particles and the support is negligible. For the Ru-richest sample, NiRu0.33 catalyst, the area under the TPR curve indicates 100% of reduction for both Ni and Ru metals. This result may seem surprising when compared with the difficulty of reduction of Ru cations for pure Ru catalyst, but, we must keep in mind that probably the strongest acidic sites of the support are already neutralized by Ni²⁺ ions in NiRu_{*x*} bimetallic catalysts, thus favouring the total reduction of Ru species. Results are compiled in Table 2, where the Ni/(Ni + Ru) molar ratios for reduced metals, Ni⁰/(Ni⁰ + Ru⁰), are also shown. The values found for samples NiRu0.89 and NiRu0.80, with very different percentages of reduced nickel, strongly suggest that these degrees of reduction of Ni species in both samples are governed by the formation of some Ni/Ru bimetallic phase with a definite composition. This phenomenon would provide an explanation about why the very well-dispersed Ni⁰ particles in these samples have migrated from the interior of the channels of the support to the external surface upon the reduction process, as deduced from TEM micrographs. The migration of Ni(II) species assisted by Ru⁰ has also been observed by Li et al. in periclase type mixed oxides, Mg(Al, Ni)O, when doped with ruthenium [18]. The same phenomenon has probably occurred for Ru-rich catalysts, NiRu0.50 and NiRu0.33, which exhibit the same Ni⁰/(Ni⁰ + Ru⁰) molar ratio.

3.6. H₂ chemisorption

Hydrogen chemisorption at 35 °C was used to estimate surface composition of the catalysts. It is necessary to point out that the contribution of Ru metal itself in the H₂ uptake on the NiRu_{*x*}

Table 2
Characterization of the metallic phase for Ni, Ru and NiRu_{*x*} bimetallic catalysts.

Catalyst	%Ni ⁰ /Ni _{<i>t</i>} ^a	Ni ⁰ /(Ni ⁰ + Ru ⁰) ^a	μmol H ₂ /g ^b	μmol H ₂ /g ^c			H/Ni ⁰ molar ratio ^b	H/Ru ⁰ molar ratio ^c	Ni ⁰ /(Ni ⁰ + Ru ⁰) _{<i>s</i>} ^e
				Peak I (T _{max} , °C) ^d	Peak II	Peak III			
Ni	30.5	1.00	35.7	0.6 (119)	8.8	1.5	0.46	–	1.00
NiRu0.89	45.1	0.78	12.2	1.3 (88)	1.0	1.2	0.12	0.05	0.90
NiRu0.80	65.4	0.72	10.4	1.9 (93)	1.6	2.1	0.08	0.04	0.84
NiRu0.67	45.9	0.48	11.7	34.1 (99)	2.1	12.7	0.16	0.42	0.26
NiRu0.50	51.2	0.34	15.7	31.5 (114)	13.7	57.1	0.25	0.26	0.33
NiRu0.33	100	0.33	13.9	74.2 (116)	28.2	69.4	0.18	0.47	0.16
Ru	33	0.00	–	14.4 (118)	1.0	40.0	–	0.53	0.00

^a From the H₂-TPR experiments.

^b From volumetric H₂ chemisorption at room temperature.

^c From H₂-TPD experiments, considering only peak I signal.

^d In brackets, temperature of the maximum.

^e Surface Ni/(Ni + Ru) molar ratio, from both r.t. and TPD-H₂ chemisorption experiments.

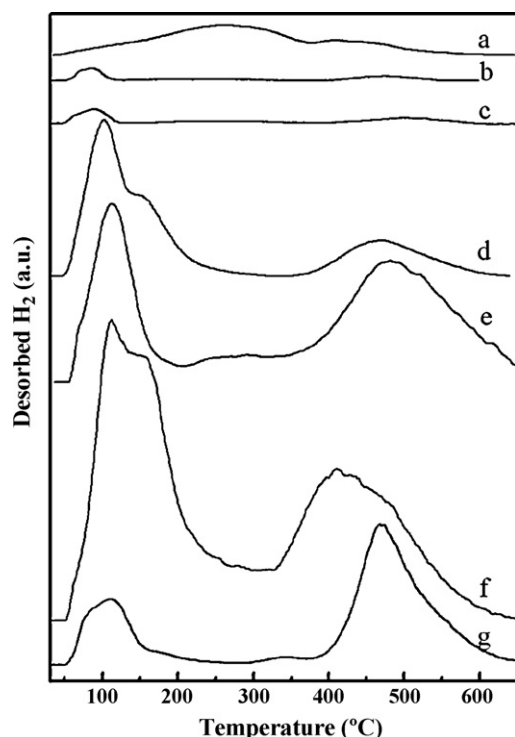


Fig. 6. H₂-TPD chromatograms for reduced catalysts: (a) Ni, (b) NiRu0.89, (c) NiRu0.80, (d) NiRu0.67, (e) NiRu0.50, (f) NiRu0.33 and (g) Ru.

catalysts must be negligible, since the pure Ru catalyst did not chemisorb any detectable amount of H₂ at this temperature, as also reported by Miyata et al. [35]. It can be a consequence of the well-established character of the activated process that exhibits the hydrogen adsorption on ruthenium [36]. So, it is assumed that at room temperature, one hydrogen atom is chemisorbed per surface nickel atom, as reported in the case of Ni/Cu alloys [37,38]. Results are depicted in Table 2. The amount of chemisorbed H₂ decreases when adding Ru to the pure Ni catalyst. Agglomeration of the metallic phase, for Ni-rich catalysts could explain the low amount of H₂ taken up; nevertheless, when the amount of Ru increases, the dispersion of the Ni-Ru phases is higher, and the amount of H₂ taken up remains almost constant.

3.7. H₂-TPD

Given that hydrogen chemisorption on metallic ruthenium is an activated process, the measurement of its surface is very commonly carried out at high temperature, that is, 100 °C or above [39]. In our case, as mentioned in Section 2, the preadsorption of hydrogen was performed at 135 °C, and prior to the TPD experiment. Chromatograms are shown in Fig. 6; the corresponding quantification is depicted in Table 2. The TPD profiles show two main peaks, centred at ca. 100 °C (peak I) and 480 °C (peak III). There is also a less defined desorption between these two peaks, with maxima between 225 and 350 °C (peak II). The lower temperature peak, peak I, is assigned to desorption of H₂ from metallic centres, while the high temperature peak, peak III, is attributed to H₂ evolved from very strong chemisorption sites on the surface of the catalyst, likely hydrogen species on the support, distant from the metallic particles, as a consequence of a spillover phenomenon. As regards to the desorption peak II, it is originated by hydrogen desorbed from chemisorption sites located at the metal-support interface [40]. The H₂-TPD profile of the pure Ni catalyst is quite different from the others, exhibiting a very broad signal with a maximum at ca. 268 °C, and only a shoulder at ca. 119 °C, indicative of a very

small quantity of H₂ chemisorbed on its metallic phase. This is in contrast to the large value measured by the room temperature volumetric method. Nevertheless, the relative large amount of H₂ chemisorbed in the metal-support interface agrees with the fact that a high metallic dispersion of Ni⁰ particles is achieved in this sample, as demonstrated by room temperature chemisorption and TEM. The reason why this sample does not chemisorb the amount of hydrogen expected is not clear. Perhaps, in our experimental conditions, fast cooling in flowing hydrogen to room temperature and subsequent purge with flowing argon, this sample did not have time enough to chemisorb hydrogen. In this sense, Boudjahem et al. also found that the amounts of chemisorbed H₂ at room temperature on Ni supported catalysts were much higher than those desorbed in the low temperature peak of the H₂-TPD experiments [41]. Also, Znak and Zielinski reported that, in the case of hydrogen preadsorption at 20 °C, the peak at 127 °C was absent in a Ni powder catalyst, while a high preadsorption temperature and extension of the time of the interaction to 24 h made it to appear [42].

For Ru catalyst, the amount of H₂ chemisorbed corroborates the very high dispersion of the metallic phase, as indicated by TEM micrographs. At the same time, it is worthy to note its great capacity to spillover hydrogen onto the support.

H₂-TPD profiles of Ni-richest bimetallic catalysts, NiRu0.89 and NiRu0.80, are also different from the others. They show a small and narrow desorption peak centred at ca. 90 °C. Furthermore, the three signals, I, II and III, are very small, which is in agreement with the lack of metal-support interactions in these catalysts, due to the agglomeration of the metallic phase and its segregation from the silica carrier. Nevertheless, the amounts of hydrogen chemisorbed by the metallic particles are very small when compared to the values obtained by the volumetric method, as happens with Ni pure catalyst, so, it seems that nickel does not chemisorb hydrogen in these catalysts.

In contrast, for the Ru-richest bimetallic catalysts, NiRu0.5 and NiRu0.33, the amount of hydrogen chemisorbed on their surfaces are much higher, indicating a better dispersion of the metallic particles, as well as much greater metal-support interactions. Since hydrogen spillover is related to the metal-support interaction and the perimeter of the interface between metal and support, these catalysts also show a very intense and broad band at high temperature (peak III), as does pure Ru catalyst. Finally, catalyst NiRu0.67, although with a peak I similar to that of Ru-rich catalysts, seems to have metal-support interactions lower than them, given the relative low intensity of its II and III signals.

From these data, it is clear that the substitution of some Ni atoms in the 3% Ni supported catalyst by Ru atoms initially agglomerates the metallic phase, but increasing the Ru loading, progressively rises the metallic dispersion of the bimetallic catalysts. This is in accordance with the positions of temperature maxima of peak I, which are located at a high temperature for Ni and Ru monometallic catalysts, ca. 118 °C, but shift smoothly to lower temperatures as the amount of Ni increases, suggesting that the agglomeration of the metallic phase provides less strong chemisorption sites for hydrogen. When sintering takes place, the electron density of the surface metal atoms increases, thus, weakening the metal-hydrogen bond [43,44].

On the other hand, by considering the amount of H₂ chemisorbed at 135 °C (peak I), it is clear that, as already discussed, for pure Ni, NiRu0.89 and NiRu0.80 catalysts, Ni⁰ does not absorb hydrogen at this temperature. On the contrary, for the rest of the NiRu_x bimetallic catalysts, the amount of H₂ chemisorbed at 135 °C (peak I) is much higher than that obtained at r.t., what would be attributable to chemisorption on Ni⁰ and Ru⁰ in a bimetallic phase. Nevertheless, if H/Ru⁰ molar ratios are calculated (where only peak I is considered, see Table 2), we find that these values are lower than that corresponding to pure Ru catalyst. This find-

Table 3
XPS data for the supported NiRu bimetallic materials, before and after reduction.

Sample	Binding energy (eV)					Ni/(Ni + Ru) molar ratio
	Ni 2p _{3/2}		Ru 3p _{3/2}			
	Ni(II)	Ni ⁰	Ru(IV)	RuO _x Cl _y	Ru ⁰ (FWHM)	
Precursors						
Ni	855.9	–	–	–	–	1.00
NiRu0.89	855.7	–	462.1	465.2	–	0.59
NiRu0.80	855.4	–	462.2	465.1	–	0.50
NiRu0.67	855.9	–	462.2	465.3	–	0.48
NiRu0.5	855.9	–	462.5	465.7	–	0.67
NiRu0.33	856.4	–	463.0	465.6	–	0.53
Ru	–	–	462.7	466.0	–	0.00
Catalysts						
Ni	855.8	852.9	–	–	–	1.00
NiRu0.89	855.9	852.7	–	–	461.4 (3.3)	0.71
NiRu0.80	855.6	852.7	–	–	461.6 (3.5)	0.62
NiRu0.67	855.8	852.8	–	–	461.8 (3.4)	0.66
NiRu0.5	855.8	852.7	–	–	462.4 (5.0) ^a	0.72
NiRu0.33	855.9	852.7	–	–	461.9 (3.9)	0.60
Ru	–	–	–	–	461.7 (4.3)	0.00

^a See text in Section 3.8, and Fig. 7.

ing suggests that, in the present experimental conditions, it is very likely that the amounts of H₂ measured on the metals are due to its chemisorption on Ru atoms only, for all catalysts. Thus, given that H₂ chemisorption at r.t. is due to surface Ni⁰ atoms, and that peak I in H₂-TPD profiles is due to surface Ru⁰ atoms, a surface Ni/(Ni + Ru) molar ratio can be calculated for these catalysts (see Table 2). The similarity of Ni/(Ni + Ru) values obtained both from H₂-TPR and chemisorption experiments indicates that this approximation is right. The results show that, as expected, the surface composition of the bimetallic catalysts changes with the added Ni/(Ni + Ru) molar ratios, and strongly suggests that certain Ni-Ru compositions are specially stable in our experimental conditions.

3.8. XPS

The XPS patterns for Ni 2p core level spectra of precursor samples show that the pure nickel precursor possesses a Ni 2p_{3/2} signal which is symmetric and sharp, with a maximum centred at

855.9 eV. This value is higher than that corresponding to pure NiO (855.0 eV [45]), and has been assigned to NiO present as small particles inside the mesopores [46]. However, the corresponding signals for bimetallic precursors are less intense and noisy, likely as a consequence of descending nickel loading. The corresponding binding energy values (Table 3) support the same idea, as already deduced from XRD data. After reduction, the Ni 2p_{3/2} signal becomes asymmetric, and can be decomposed into two contributions, one centred at ca. 855.8 eV and another one at ca. 852.8 eV, respectively (Fig. 7). The peak at 855.8 eV could be associated with the very small crystallites of remaining NiO located on the walls of the mesostructure; while the other peak at ca. 852.8 eV corresponds to Ni⁰ species. For bimetallic NiRu catalysts, the maximum of this peak is slightly shifted to lower B.E. values, compared to the pure Ni catalyst, what could be due to differences in the metal–support interactions, but also as consequence of the interaction of Ni⁰ and Ru⁰ atoms. Nevertheless, this last possibility seems unlikely, since the contribution of such an interaction to the core level shift is minimal, well within

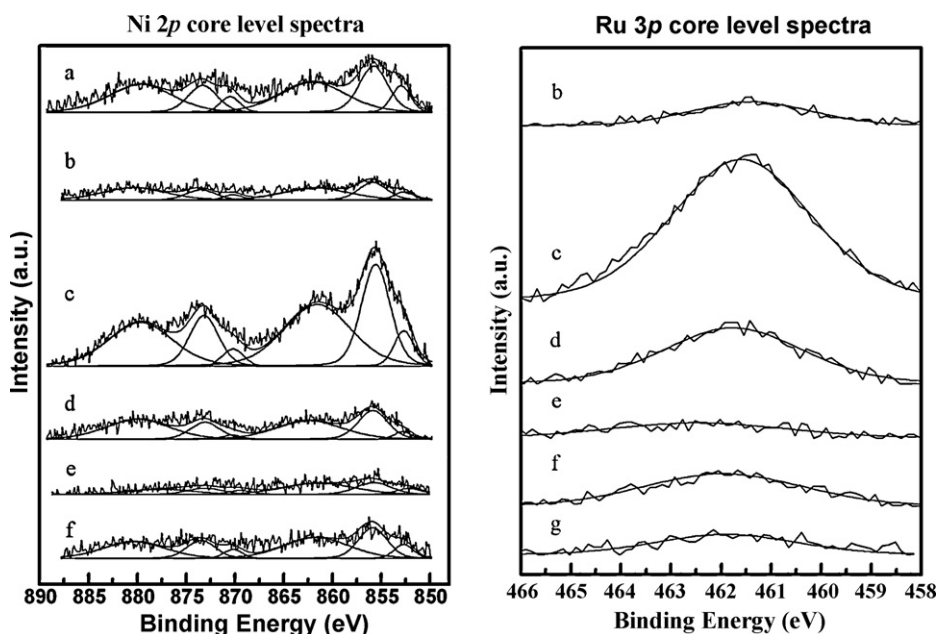


Fig. 7. Ni 2p and Ru 3p core level spectra for reduced catalysts: (a) Ni, (b) NiRu0.89, (c) NiRu0.80, (d) NiRu0.67, (e) NiRu0.50, (f) NiRu0.33 and (g) Ru.

the experimental error [47,48]. The peak areas of Ni⁰ signals were much smaller than that of NiO signals. This may indicate that only a small fraction of NiO was reduced, in contrast to what is deduced from H₂-TPR experiments. We must keep in mind that before XPS analysis, the reduced samples were shortly exposed to the air while moved from the reactor to the analysis chamber. So, this low fraction of reduction could be the result of the reaction of dispersed Ni⁰ with oxygen at room temperature. Furthermore, it is well known that, when Ni⁰ are formed, the atoms located in the interior of the particles, can hardly be detected by this technique [49].

Ru species were analysed by recording the Ru 3p spectrum of samples. The Ru 3p_{3/2} signals for catalyst precursors are slightly asymmetric, and can be decomposed into two contributions: a main one with its maximum centred at ca. 462.1–463.1 eV, that can be assigned to the presence of Ru(IV) species, and a small shoulder at higher binding energies, between 465.1 and 466.0 eV, which is attributed to the presence of RuO_xCl_y compounds, most likely with Ru atoms in +IV oxidation state [50], which corroborates that Ru in our pristine salt is mostly in the +IV oxidation state, as already mentioned.

Recorded spectra for reduced catalysts are also depicted in Fig. 7. The Ru 3p_{3/2} signals are now symmetric, with their maxima between 461.4 and 461.9 eV, which, according to the literature [50], correspond to the binding energy of Ru⁰. Nevertheless, the FWHM of the signals of more than 3.3 eV could suggest the presence of ruthenium atoms in more than one oxidation state. This is the case for pure Ru catalyst, the signal being the result of the presence of Ru⁰ and Ruⁿ⁺ species, as deduced from H₂-TPR experiments. Besides, this catalyst shows the broadest signal. On the other hand, for NiRu_x bimetallic catalysts, very high metal reduction degrees are likely, thus these broad signals must be due to different chemical environments for Ru⁰ atoms originated by metal–support interactions, as well as Ni–Ru interactions (note that these Ru 3p signals are narrower than that for pure Ru catalyst, with the exception of NiRu0.50 catalyst, with a very low intensity and noisy signal). Furthermore, before XPS analysis, the reduced samples were shortly exposed to the air, and so, these broaden signals could also be the result of some surface RuO₂ [51].

On the other hand, it is worthy to point out that Ru 3p signals become less intense and noisier as the Ru content increases. Considering that XPS is essentially a surface technique, most of the metallic particles located in the porous structure of the support, with wall thickness of ca. 50 Å, are not detected [52]. This means that, at least for Ru-rich samples, NiRu0.33 and NiRu0.50, a great fraction of the metal has entered into the tubular channels of the support, as also happens with pure Ru catalyst. On the contrary, NiRu0.80 catalyst, with still a low percentage of Ru, shows the most intense Ru 3p signal, which indicates that almost all the metallic particles were formed on the external surface of the support, as has been already described.

Concerning the surface chemical composition, in Fig. 8 the Ni/(Ni + Ru) surface molar ratios for catalyst precursors (from XPS chemical analysis) have been plotted versus the corresponding bulk values. Surprisingly, all surface values differ from those of bulk values in such a way that the former ones are around a constant value of 0.55. As NiO is a basic oxide, and RuCl₃ is an acid salt, and given that the respective cations sizes are very similar [53], it is likely that an interaction between both solids has happened during the impregnation and subsequent drying process, perhaps giving rise to any kind of mixed compound, and thus, altering the Ru distribution on the support surface, and hence, the Ni/(Ni + Ru) surface molar ratios. It means that, when the amount of NiO present on the support before impregnation with the Ru salt is small, as in samples NiRu0.50 and NiRu0.33, a great fraction of Ru ions has entered into the mesopores of the support. The opposite must have happened for Ni-rich precursors, where a higher fraction of Ru cations seems

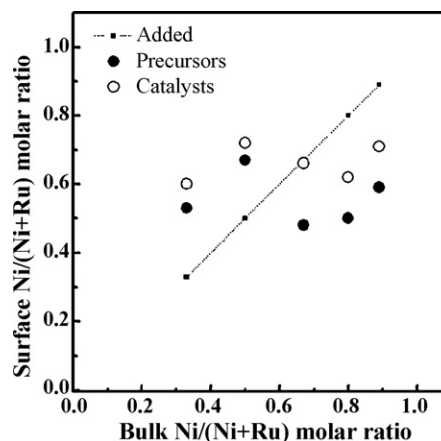


Fig. 8. Surface Ni/(Ni + Ru) molar ratio, as measured by XPS analysis, for catalyst precursors and reduced catalysts, as a function of bulk composition.

to remain on the external surface of the support, thus giving rise to surface Ni/(Ni + Ru) molar ratio values lower than those of bulk ones. An important consequence of this may be the fact that probably a close interaction between the two metal cations, Ni²⁺ and Ruⁿ⁺, occurs, already before the reduction process, which would be reflected in the H₂-TPR profiles, as discussed.

As regards the Ni/(Ni + Ru) molar ratio values for reduced samples, also shown in Fig. 8, they are slightly higher than those corresponding to the non-reduced ones, and again, they do not follow the bulk values, but oscillate around a mean value of 0.66. This apparent contradiction can be explained by taking into account that in low loading-Ni catalysts, Ni atoms are mainly forming the metallic particles located on the external surface of the support, which are well detected by XPS technique, and, furthermore, with the same composition as those present in high loading-Ni catalysts. This implies that the metallic particles situated within the pores of the support, not detectable by XPS, must be Ru-enriched, which corroborates the formation of two or more bimetallic phases of special stability in our series of catalysts.

Finally, it has been reported that Ru catalysts derived from the reduction of RuCl₃ retain residual chlorine after reduction with hydrogen [31]. However, no XPS peaks for chloride atoms are found in the reduced materials, indicating that this element has been completely removed upon the reduction process, in accordance with results reported by others [54].

3.9. NH₃-TPD

The NH₃-TPD profile for the SBA-15 support (Fig. 9) exhibits one small and well-defined, almost symmetric desorption peak, with its maximum centred at 136 °C, which corresponds to weak acid sites. After nickel incorporation onto the support, this peak shifts to higher temperature, 151 °C, while becomes asymmetric, with a pronounced tail which extends to high temperature; only when the temperature ramp is stopped at 400 °C, the signal falls to the base line again. This profile clearly indicates the broad distribution of acid centres strengths, those in the weak range being the more abundant. Moreover, the total number of acid sites of the catalyst increases in comparison to that of the support (Table 1). The nickel modification over the acidity of the support has two different causes. The nickel species could cover some of the acid sites (both Bronsted and Lewis acid sites), causing the decrease of the total acid sites; but, on the other hand, the co-ordinately unsaturated nickel cations could serve as a kind of new Lewis acid centres, which compensate the original acid sites being covered. In the present case, the compensating effect of the Ni species overrides the covering

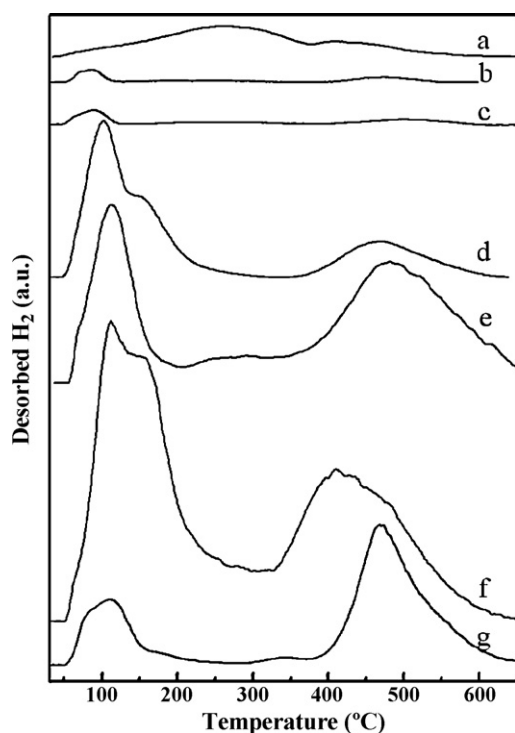


Fig. 9. NH_3 -TPD patterns for reduced catalysts: (a) Ni, (b) NiRu0.89, (c) NiRu0.80, (d) NiRu0.67, (e) NiRu0.50, (f) NiRu0.33, (g) Ru, and (h) SBA-15 support.

one, which causes an increase of the total acid sites [55]. The low degree of Ni reduction explains this great increment of the total acidity in comparison with the support. This TPD pattern is followed by the other catalysts, with only slight modifications, which can be attributed to ruthenium content and the dispersion of the metallic phase. Thus, for Ni-rich catalysts (NiRu0.89 and NiRu0.80) the ammonia desorption peak is narrower, and less intense, while for the rest of catalysts, this peak gets broader and more intense as the ruthenium content and metallic dispersion increase. These data are in accordance with those reported by other authors [56], and are attributed to the higher tendency of Ru to adsorb ammonia molecules. In fact, a good correlation of the total amount of desorbed ammonia and the surface Ru^0 content of the bimetallic catalysts (calculated by chemisorption methods) is found, which clearly indicates that the surface Ru^0 is responsible, at least, of the major part of the ammonia chemisorbed by the bimetallic NiRu catalysts.

3.10. Catalytic results

This family of NiRu bimetallic catalysts was evaluated in the hydrogenation of acetonitrile in the gas phase at atmospheric pressure. Under our experimental conditions, only the primary, secondary and tertiary amines have been obtained (referred to as EA, DEA and TEA, respectively).

Table 4

Catalytic performance of Ni, and bimetallic NiRu catalysts, in the hydrogenation of acetonitrile.

Catalyst	Conversion (mol%)	TOF_{Ni} (s^{-1})	Selectivity (mol%)			EA yield (%)
			EA	DEA	TEA	
Ni	38.7	0.73 (1.0) ^a	57.0	33.9	9.1	22.1
NiRu0.89	30.6	1.69 (2.3)	60.9	27.8	11.3	18.6
NiRu0.80	27.3	1.78 (2.4)	60.4	28.1	11.5	16.5
NiRu0.67	36.1	2.08 (2.8)	59.4	27.8	12.8	21.4
NiRu0.50	40.2	1.73 (2.3)	59.4	30.9	9.7	23.9
NiRu0.33	45.0	2.18 (3.0)	58.4	30.5	11.1	26.3

^a In brackets, relative values, $\text{TOF}_{\text{Ni}}/(\text{TOF}_{\text{Ni}}$ for pure Ni catalyst).

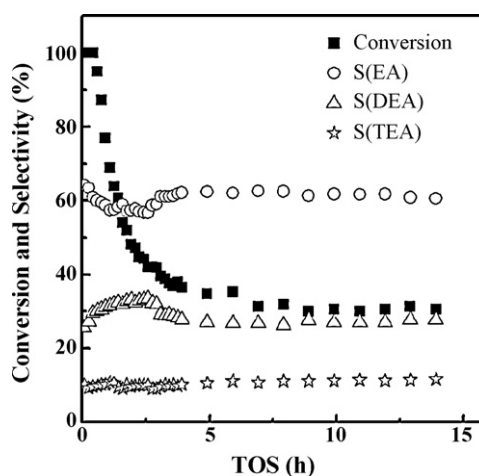


Fig. 10. Conversion and selectivity changes for NiRu0.89 catalyst, as a function of time on stream, for the hydrogenation of acetonitrile in the gas phase at 135 °C and atmospheric pressure ($F/W = 121 \mu\text{mol CH}_3\text{CN g}_{\text{cat}}^{-1} \text{s}^{-1}$; $\text{H}_2:\text{CH}_3\text{CN}$ molar ratio = 20).

The changes in acetonitrile conversion as well as in selectivities with time on stream (TOS) for sample NiRu0.89 are shown in Fig. 10. In all cases, with the exception of Ru catalyst, which was inactive, the initial conversion of acetonitrile was 100%, but, after a deactivation period, the steady state was achieved. It is worthy to note that pure Ru catalysts employed by other authors were active at similar reaction temperatures, but with very low conversion values [57].

Table 4 depicts the values of acetonitrile conversion and the selectivities towards the amines for Ni and NiRu bimetallic catalysts in the steady state. Conversion% values are low, between 30% and 45%, what is consistent with the reaction mechanism proposed by Huang and Sachtler [12,58], after which, desorption of a product molecule must be assisted by the chemisorption of an acetonitrile molecule, giving rise to an overall reaction



for the primary amine production [59].

The observed conversion% values change as a function of catalysts composition, decreasing upon the addition of small amounts of Ru, in comparison with the pure Ni catalyst, but increasing when larger amounts of Ni have been substituted for Ru, giving rise to higher values than that observed for the pure Ni catalyst. Concerning the selectivity values towards EA, they decrease monotonically as the amount of Ru in the bimetallic catalysts increases, although, in all cases, they are higher than that for pure Ni catalyst. As a result, higher EA yields are achieved for Ru-rich catalysts. These values are much higher than those reported by Huang et al. [57] for pure Ru supported on different zeolites: at conversion values between 2% and 4%, they describe selectivity values towards EA of ca. 71–81%, when a reaction temperature of 75 °C was employed, but, at conversion values of 8.6%, a selectivity of 46% towards EA was

reported, when the reaction temperature was 110 °C. Furthermore, when Ru was supported on alumina, the catalyst was not active at 75 °C; only at 125 °C it exhibited an acetonitrile conversion of 15.3%, with selectivity towards EA of 24.2%. On the other hand, our results are similar to those reported by other authors [15,60], who also found an enhanced catalytic activity in Ni-Fe bimetallic catalysts, although the selectivity pattern remained unchanged.

Although the pure Ru catalyst was inactive in the hydrogenation reaction, it is possible that it becomes active when alloyed with Ni atoms. To explore this possibility, a turnover frequency of surface Ni⁰ atoms (referred to as TOF_{Ni}), calculated as acetonitrile moles converted per exposed Ni⁰ atom and second, has been calculated (Table 4). These values are very similar for all the bimetallic catalysts, and 2.3–3.0 times higher than that of pure Ni catalyst. This clearly indicates that the active sites are Ni⁰ atoms, and that their specific activity (TOF_{Ni}) has been enhanced by direct interaction with Ru atoms, irrespective of other factors that might also affect, although in a lesser extent, as the dispersion. Furthermore, these data rule out any structure demanding character of the hydrogenation reaction, as proposed by some authors [61]. Since these TOF_{Ni} values remain almost constant for the bimetallic catalysts, that is, with the surface Ni⁰ concentration, the dilution of these Ni⁰ atoms with non-active Ru⁰ atoms has no effect on the Ni⁰ specific catalytic activity, and so, an ensemble effect is dismissed, i.e., the catalytic centres seem to be monoatomic surface Ni⁰ sites, as also reported by others [15]. This enhancement of Ni specific activity in the hydrogenation of different nitriles by direct interaction with other metals have already been reported by many authors [62,13]; some of them attributed this finding to electronic effects (the so-called *ligand effect*), i.e., to an electron transfer from promoter atoms to the active Ni⁰ atoms, thus changing the electronic properties of nickel atoms.

To analyse this possibility, it is necessary to briefly review the chemisorption properties of the acetonitrile molecule. The nitrile group contains a heteronuclear triple bond with occupied σ -non-bonding and doubly degenerated π -bonding orbitals and doubly degenerated π^* -orbitals. Acetonitrile has two possible adsorption geometries, either perpendicular to the surface through the nitrogen lone pair or parallel to the surface through the π system. When an end-on coordination via the N atom takes place, an increase in the strength of C–N bonding is found compared to the gaseous acetonitrile molecule. In this case, back donation from the metal orbitals to the π^* orbitals of the nitrile group is negligible. In contrast, in the side-on bonded coordination, a forward donation of a pair of electrons from the bonding π orbitals of the nitrile group to the metal atoms takes place, while back donation from metal atom orbitals to the unoccupied antibonding molecular orbitals π^* happens, resulting in a reduction of C–N bond order. Thus, the reactivity of the nitrile group is directly related to the adsorption mode [61]. According to this, the parallel chemisorption seems to be the best form for reaction with hydrogen [63].

Therefore, increased back donation ability of Ni⁰ in the Ni-Ru bimetallic particles would favour the CN bond weakening, thus leading to higher TOF_{Ni} values for NiRu bimetallic catalysts in the hydrogenation reaction, as experimentally observed.

Nevertheless, literature dealing with Ni electronic properties in mixed Ni-Ru phases is not clear [64]. On the other hand, experimental techniques employed in the present work suggest that the electron-richness of the surface of metallic phases increases as the Ni-content is raised. Therefore, the activation of the acetonitrile molecule should be easier with increasing amounts of Ni, and thus, higher TOF_{Ni} values would be expected, contrary to what is experimentally found. Therefore, our catalytic results are not explained by considering electronic effects. So, given that it seems that for Ru–Ni alloys the electronic structure of Ni atoms varies only marginally by alloying [65], and that both components also preserve their individ-

uality in alloys, as also happens with Ni–Cu alloys [66], the observed promoting effect might have some other cause.

Taking into account the strong interaction of ammonia molecules with Ru⁰ atoms, as shown by NH₃-TPD experiments, it is possible that surface Ru⁰ atoms adjacent to Ni⁰ atoms can attract the electron pair from the non-bonding orbital on the N atom of the nitrile molecule [15], thus favouring the anchorage of the CN group to the active Ni⁰ ones, and hence, its activation. Furthermore, these Ru⁰ atoms, could also stabilize some reaction intermediates, such as the nitrone, CH₃–CH₂–N=, doubly bonded to the surface. It is known that Ru atoms are better than Ni ones in establishing multiple bonds [67]. This would supply more activated forms for the last hydrogenation step, before desorption of EA, and/or for subsequent condensation steps.

Lastly, another possibility is that Ru⁰ atoms can enhance desorption of product molecules. Here, it is important to take into account the reaction mechanism proposed by Huang and Sachtler [12], in which desorption of a product molecule is proposed to be the rate-limiting step: the release of a strongly held intermediate from the surface is assisted by the interaction with another colliding nitrile molecule, which suffers a dissociative H–C chemisorption, thus acting simultaneously as hydrogen donor in the last hydrogenation step of a final product. In this sense, Ru is known to be a very good catalyst for C–H bond dissociation, as proved by its catalytic activity in reactions such as methane conversion [68], or α,α -bonding of alkanes [67]. Hence, the amines formed in the Ni⁰ catalytic centres may be easily transferred to adjacent Ru⁰ atoms, given its great affinity for N-containing species, and finally desorbed by an enhanced acetonitrile dissociative chemisorption, thus regenerating the catalytic Ni⁰ site. The number of such catalytic sites, exposed adjacent Ni⁰–Ru⁰, must be a function of surface composition. Besides, if the reaction rate is controlled by desorption of products from one M⁰ atom in the way already explained, then, the catalytic centre responsible for this step would be monoatomic, as observed experimentally.

4. Conclusions

The bimetallic NiRu catalysts exhibited a synergism effect for the gas phase hydrogenation of acetonitrile, in comparison with Ni and Ru monometallic catalysts. This synergism seems to be the result of intimate contact between both metallic atoms, as a consequence of some nanoalloy/s formation. Adjacent Ni⁰–Ru⁰ sites could be responsible for the catalytic performance observed, likely by a better desorption of hydrogenation products, as proposed in the literature. Nevertheless, results also show the need for a better control of the dispersion of the metallic phases, in order to enhance conversion values. Thus, only well-dispersed metallic phases gave high catalytic acetonitrile conversions as well as high ethylamine yields. Given that the specific activity per Ni⁰ atom has been greatly enhanced for all Ni/(Ni + Ru) compositions, it seems desirable to modify the synthetic route to attain well-dispersed Ni-rich Ni–Ru alloys. On the other hand, selectivity patterns for bimetallic catalysts remained almost equal to that of pure Ni catalyst.

Acknowledgements

We gratefully acknowledge the funding of this work by the Junta de Andalucía (Spain) Excellence Project P06-FQM-01661.

References

- [1] B. Chen, U. Dingerdissen, J.G.E. Krauter, H.G.J. Lansink Rotgerink, K. Möbus, D.J. Ostgard, P. Panster, T.H. Riermeier, S. Seebald, T. Tacke, H. Trauthwein, Appl. Catal. A: Gen. 280 (2005) 17–46.
- [2] P.N. Rylander, Catalytic Hydrogenation in Organic Synthesis, Academic Press, New York, 1979.

- [3] J. Volf, J. Pasek, in: L. Cerveny (Ed.), *Catalytic Hydrogenation*, Elsevier, Amsterdam, 1986, pp. 105–144.
- [4] C. De Bellefon, P. Fouilloux, *Catal. Rev. Sci. Eng.* 36 (1994) 459–506.
- [5] Y. Huang, W.M.H. Sachtler, *Appl. Catal. A: Gen.* 182 (1999) 365–378.
- [6] M.J.F.M. Verhaak, A.J. van Dillen, J.W. Geus, *Catal. Lett.* 26 (1994) 37–53.
- [7] F. Medina, R. Dutartre, D. Tichit, B. Coq, N.T. Dung, P. Salagre, J.E. Sueiras, *J. Mol. Catal. A: Chem.* 119 (1997) 201–212.
- [8] P. Braos-García, P. Maireles-Torres, E. Rodríguez-Castellón, A. Jiménez-López, *J. Mol. Catal. A: Chem.* 168 (2001) 279–287.
- [9] A. Infantes-Molina, J. Mérida-Robles, P. Braos-García, E. Rodríguez-Castellón, E. Finocchio, G. Busca, P. Maireles-Torres, A. Jiménez-López, *J. Catal.* 225 (2004) 479–488.
- [10] J.L. Dallons, A. Van Gysel, G. Jannes, in: W. Pascoe (Ed.), *Catalysis of Organic Reactions*, Dekker, New York, 1992, p. 93.
- [11] Y. Huang, W.M.H. Sachtler, *J. Phys. Chem. B* 102 (1998) 6558–6565.
- [12] Y. Huang, W.M.H. Sachtler, *J. Catal.* 184 (1999) 247–261.
- [13] Y. Huang, W.M.H. Sachtler, *J. Catal.* 188 (1999) 215–225.
- [14] M. Arai, T. Ebina, M. Shirai, *Appl. Surf. Sci.* 148 (1999) 155–163.
- [15] G.D. Yadav, M.R. Kharkara, *Appl. Catal. A: Gen.* 126 (1995) 115–123.
- [16] R. Ferrando, J. Jellinek, R.L. Johnston, *Chem. Rev.* 108 (3) (2008) 845–910.
- [17] J.B. Liu, X.Y. Li, B.X. Liu, *Solid State Commun.* 121 (2002) 375–379.
- [18] D. Li, I. Atake, T. Shishido, Y. Oumi, T. Sano, K. Takehira, *J. Catal.* 250 (2007) 299–312.
- [19] J.M. Rynkowski, T. Paryczak, M. Lenik, *Appl. Catal. A: Gen.* 126 (1995) 257–271.
- [20] J. Phillips, J. Weigle, M. Herskowitz, S. Kogan, *Appl. Catal. A: Gen.* 173 (1998) 273–287.
- [21] S.M. da Silva, J. Phillips, *J. Mol. Catal.* 94 (1994) 97–116.
- [22] M. Gómez-Cazalilla, J.M. Mérida-Robles, A. Gurbani, E. Rodríguez-Castellón, A. Jiménez-López, *J. Solid State Chem.* 180 (2007) 1130–1140.
- [23] D.J. Lensveld, J.G. Mesu, A.J. van Dillen, K.P. de Jong, *Microporous Mesoporous Mater.* 44–45 (2001) 401–407.
- [24] S. Brunauer, P.H. Emmet, E. Teller, *J. Am. Chem. Soc.* 60 (1938) 309–319.
- [25] L. Jellinek, E.sz. Kováts, *Langmuir* 10 (1994) 4225–4231.
- [26] A. Galarneau, D. Desplandier, R. Dutartre, F. Di Renzo, *Microporous Mesoporous Mater.* 27 (1999) 297–308.
- [27] B. Chandret, S. Sabo-Etienne, in: R.B. King (Ed.), *Encyclopedia of Inorganic Chemistry*, Wiley, Chichester, 1994, pp. 3515–3516.
- [28] L. Jinxiang, Y. Lixin, G. Shuiying, H. Lijuan, T. Renyuan, L. Dongbai, *Thermochim. Acta* 123 (1988) 121–133.
- [29] P. Betancourt, A. Rives, R. Hubaut, C.E. Scott, J. Goldwasser, *Appl. Catal. A: Gen.* 170 (1998) 307–314.
- [30] D. Eliche-Quesada, E. Rodríguez-Castellón, A. Jiménez-López, *Microporous Mesoporous Mater.* 99 (2007) 268–278.
- [31] V. Mazzieri, F. Coloma-Pascual, A. Arcoya, P.C. L'Argentière, N.S. Fígoli, *Appl. Surf. Sci.* 210 (2003) 222–230.
- [32] J. Li, G. Lu, K. Li, W. Wang, *J. Mol. Catal. A: Chem.* 221 (2004) 105–112.
- [33] M. Cerro-Alarcón, A. Guerrero-Ruiz, I. Rodríguez-Ramos, *Catal. Today* 93–95 (2004) 395–403.
- [34] C. Crisafulli, S. Scirè, R. Maggiore, S. Minicò, S. Galvagno, *Catal. Lett.* 59 (1999) 21–26.
- [35] T. Miyata, M. Shiraga, D. Li, I. Atake, T. Shishido, Y. Oumi, T. Sano, K. Takehira, *Catal. Commun.* 8 (2007) 447–451.
- [36] K.C. Taylor, *J. Catal.* 38 (1975) 299–306.
- [37] W.M.H. Sachtler, P. van der Plank, *Surf. Sci.* 18 (1969) 62–79.
- [38] J.H. Sinfelt, J.L. Carter, D.J.C. Yates, *J. Catal.* 24 (1972) 283–296.
- [39] H.Y. Lin, Y.W. Chen, *Thermochim. Acta* 419 (2004) 283–290.
- [40] F.S. Modica, J.T. Miller, B.L. Meyers, D.C. Koningsberger, *Catal. Today* 21 (1994) 37–48.
- [41] A.G. Boudjahem, S. Monteverdi, M. Mercy, M.M. Bettahar, *J. Catal.* 221 (2004) 325–334.
- [42] L. Znak, J. Zielinski, *Langmuir* 22 (2006) 8758–8763.
- [43] J.A. Dalmon, C. Mirodatos, *J. Mol. Catal.* 25 (1984) 161–172.
- [44] B.L. Mojet, J.T. Miller, D.E. Ramaker, D.C. Koningsberger, *J. Catal.* 186 (1999) 373–386.
- [45] P. Salagre, J.L.G. Fierro, F. Medina, J.E. Sueiras, *J. Mol. Catal. A: Chem.* 106 (1996) 125–134.
- [46] R. Moreno-Tost, J. Santamaría-González, P. Maireles-Torres, E. Rodríguez-Castellón, A. Jiménez-López, *J. Mater. Chem.* 12 (2002) 3331–3336.
- [47] J.A. Rodríguez, R.A. Campbell, D.W. Goodman, *J. Phys. Chem.* 94 (1990) 6936–6939.
- [48] R.A. Campbell, J.A. Rodríguez, D.W. Goodman, *Surf. Sci.* 256 (1991) 272–280.
- [49] J.A. Anderson, L. Daza, J.L. Fierro, M.T. Rodrigo, *J. Chem. Soc. Faraday Trans.* 89 (19) (1993) 3651–3657.
- [50] J.F. Moulder, W.F. Stickle, P.E. Sobol, K.D. Bomben, in: J. Chastain (Ed.), *Handbook of X-ray Photoelectron Spectroscopy*, PerkinElmer, Minneapolis, 1992.
- [51] P.G.J. Koopman, A.P.G. Kieboom, H. van Bekkum, *Colloids Surf.* 3 (1981) 1–12.
- [52] P. Reyes, M.E. König, G. Pecci, I. Concha, M. López-Granados, J.L.G. Fierro, *Catal. Lett.* 46 (1997) 71–75.
- [53] N.N. Greenwood, A. Ernschaw, *Chemistry of the Elements*, second ed., Butterworth-Heinemann, Oxford, 1998.
- [54] M.G. Cattania, F. Parmigiani, V. Ragaini, *Surf. Sci.* 211/212 (1989) 1097–1105.
- [55] K. Fang, J. Ren, Y. Sun, *J. Mol. Catal. A: Chem.* 229 (2005) 51–58.
- [56] D. Eliche-Quesada, J.M. Mérida-Robles, E. Rodríguez-Castellón, A. Jiménez-López, *Appl. Catal. A: Gen.* 279 (2005) 209–221.
- [57] Y. Huang, V. Adeeva, W.M.H. Sachtler, *Appl. Catal. A: Gen.* 196 (1) (2000) 73–85.
- [58] Y. Huang, W.M.H. Sachtler, *J. Catal.* 190 (2000) 69–74.
- [59] Y. Huang, W.M.H. Sachtler, *Stud. Surf. Sci. Catal.* 130 (2000) 527–532.
- [60] P.S. Kumbhar, M.R. Kharkar, G.D. Yadav, R.A. Rajadhyaksha, *J. Chem. Soc., Chem. Commun.* (1992) 584–586.
- [61] M. Arai, Y. Takada, Y. Nishiyama, *J. Phys. Chem. B* 102 (1998) 1968–1973.
- [62] M. Wang, H. Li, Y. Wu, J. Zhang, *Mater. Lett.* 57 (2003) 2954–2964.
- [63] B. Bigot, F. Delbecq, A. Milet, V.-H. Peuch, *J. Catal.* 159 (1996) 383–393.
- [64] J.A. Rodríguez, R.A. Campbell, D.W. Goodman, *J. Vac. Sci. Technol. A* 9 (3) (1991) 1698–1702.
- [65] J.R. Kitchin, J.K. Norskov, M.A. Barteau, J.G. Chen, *Phys. Rev. Lett.* 93 (15) (2004) 156801–156804.
- [66] M. Araki, V. Ponec, *J. Catal.* 44 (1976) 439–448.
- [67] E.H. van Broekhoven, V. Ponec, *J. Mol. Catal.* 25 (1984) 109–118.
- [68] L. Guzzi, K.V. Sarma, L. Borkó, *React. Kinet. Catal. Lett.* 68 (1) (1999) 95–104.